Artificial and natural radionuclides in cryoconite as tracers of supraglacial dynamics

Giovanni Baccolo[1,2*], Massimiliano Nastasi[2,3], Dario Massabò[4,5], Caroline Clason[6], Biagio Di Mauro[1], Elena Di Stefano[1,2,7], Edyta Łokas[8], Paolo Prati[4,5], Ezio Previtali[2,3], Nozomu Takeuchi[9], Barbara Delmonte[1,2], Valter Maggi[1,2]

1. Environmental and Earth Sciences Department, University of Milano-Bicocca, P.za della Scienza n.1, Milano, 20126, Italy
2. INFN section of Milano-Bicocca, P.za della Scienza n.3, Milano, 20126, Italy
3. Physics Department, University of Milano-Bicocca, P.za della Scienza n.3, Milano, 20126, Italy
4. Physics Department, University of Genova, Genova, 16146, Italy
5. INFN section of Genova, Genova, 16146, Italy
6. School of Geography, Earth and Environmental Sciences, University of Plymouth, Plymouth, PL48AA, UK
7. Department of Physical, Earth and Environmental Sciences, University of Siena, Siena, 53100, Italy
8. Department of Mass Spectrometry, Institute of Nuclear Physics Polish Academy of Sciences, Kraków, 31-342, Poland
9. Department of Earth Sciences, Graduate School of Science, Chiba University, Chiba, Japan

* corresponding author: giovanni.baccolo@unimib.it

Abstract

Cryoconite, a sediment found on the surface of glaciers, is known for its ability to accumulate radionuclides. New data on cryoconite from the Morteratsch glacier (Switzerland) are presented with the aim to shed light on the mechanisms that control the distribution of radioactivity in cryoconite. Among the many radionuclides detected in our samples, we have identified ^{108m}Ag, an artificial species which has never been observed in terrestrial environments before. This finding supports that cryoconite has an extraordinary ability to accumulate radioactivity. Our results also show that the radioactivity of cryoconite is far from uniform. Both the absolute amount of radioactivity and the relative contribution of single radionuclides is highly variable in samples from the Morteratsch glacier. To investigate the processes responsible for such variability, we have explored the correlation between radionuclides, organic and inorganic carbon fractions and the morphological features of cryoconite deposits. We have found that the degree to cryoconite is connected with supraglacial hydrology is particularly important, since it strongly influences the accumulation of radionuclides in cryoconite. Cryoconite holes connected with supraglacial channels is rich in cosmogenic ^{7}Be; in contrast, poorly connected deposits are rich in artificial fallout radionuclides and elemental carbon. The very different half-lives of ^{7}Be and artificial radionuclides allowed us to discuss our findings in relation to the age and maturity of cryoconite deposits, highlighting the potential use of radionuclides to investigate hydrological supraglacial processes and material cycling at the surface of glaciers.

Keywords

Cryoconite; Environmental Radioactivity; ^{7}Be; Supraglacial Processes; Glacial Hydrology; Artificial Radionuclides

1. Introduction

Radioactivity is a versatile tool in Earth Sciences, with many diverse applications. When focusing on the Earth's surface, common uses of radioactivity concern the study of fallout radionuclides (FRN) to develop chronologies for recent sediments (Appleby, 2008) and to investigate erosion and sedimentation processes (Mabit et al., 2008). One research field that owes much to radioactivity is glaciology. The first glaciological applications of radioactivity date back to the 1960s, when pioneering studies on the development of age scales for snow and ice through the detection of FRN appeared (Picciotto and Wilgain, 1963; Crozaz et al., 1964). Since then, the analysis of the decay rate of natural fallout ^{210}Pb and the identification of radioactive spikes corresponding to nuclear accidents and test explosions have become a routine procedure to date the upper layers of ice cores (Eichler et al., 2000; Clemenza et al., 2012). This has been possible because snow and ice, being atmospheric in origin, record the atmospheric history of a given region (Preunkert & Legrand, 2013), radioactive fallout included (Pinglot et al., 1994). But glaciers are not isolated systems, they are not exclusively a sink for fallout material, since through ablation and melt part of the airborne matter accumulated into glaciers is released in the downstream environment. This is now widely recognized, and glaciers are no longer considered simply as repositories, but also as secondary sources for many impurities of ecological importance (Gerringa et al., 2012), including pollutants (Bogdal et al., 2009; Rizzi et al., 2019) and radionuclides (Łokas et al., 2017; Owens et al., 2019).

Within this context radioactivity plays an important role. In recent years it has been observed that before being released in pro-glacial areas, FRN stored in glaciers are accumulated at their surface in association with cryoconite (Tieber et al., 2009; Łokas et al., 2016; Baccolo et al., 2019). Cryoconite is the dark sediment that forms at the surface of many glaciers across the global cryosphere during the melt season. It is mostly composed of fine mineral sediments, but it is also rich in organic matter, owing to notable microbial activity (Hodson et al., 2010). Its dark color, related to high organic content (Takeuchi, 2002), impacts the radiative properties of ice, enhancing its melt (Di Mauro et al., 2017; Li et al., 2019). The abundance of organic matter and the interaction with meltwater makes cryoconite a natural filter, capable of accumulating diverse impurities originally present in ice and mobilized through meltwater (Baccolo et al., 2017). In particular, it has been observed that pollutants are efficiently accumulated in cryoconite, including heavy metals (Nagatsuka et al., 2010; Łokas et al., 2016; Baccolo et al., 2017; Huang et al., 2019), organic compounds (Li et al., 2017; Weiland-Bräuer et al., 2017), pesticides (Ferrario et al., 2017) and radionuclides (Tieber et al., 2009; Łokas et al., 2016; Baccolo et al., 2019).

Despite early evidence about the ability of cryoconite to accumulate radionuclides, Tieber and coauthors (2009) were the first to present a quantitative radioecological characterization of cryoconite. They showed that the activity concentration of single radionuclides in cryoconite from an Austrian glacier exceeded 100,000 Bq Kg^{-1} (Tieber et al., 2009). Similar evidence was reported in

following years for other geographic contexts (Łokas et al., 2016; Baccolo et al., 2019; Owens et al., 2019), confirming that cryoconite accumulates FRN with unprecedented efficiency. The typical activities observed in cryoconite are orders of magnitude higher than those characterizing the matrices usually adopted for environmental radioactivity monitoring, such as lichens and mosses. In terms of radioactive contamination, only samples from nuclear accident and test explosion sites are comparable to or exceed cryoconite (Baccolo et al., 2019). Recent works have suggested that the ability of cryoconite to retain and accumulate radionuclides depends on its composition, which is rich in organic matter, and on its interaction with the meltwater that flows at the surface of glaciers during summer (Łokas et al., 2016; Baccolo et al., 2019). Meltwater is in fact the means by which the impurities deposited in the past on the glacier, and subsequently preserved in snow and ice layers, come into contact with cryoconite (Baccolo et al., 2019). Studies have shown that cryoconite accumulates both natural FRN, such as ^{210}Pb and ^{7}Be, and anthropogenic FRN, such as ^{137}Cs, Pu and Am isotopes, which were released in the environment as a consequence of nuclear accidents, test explosions and atmospheric re-entries of nuclear powered satellites (Tieber et al., 2009; Baccolo et al., 2019; Łokas et al., 2019). After being accumulated at the surface of glaciers, cryoconite and its radioactive content are released by glaciers in association with meltwater. Preliminary results have shown that a fraction of cryoconite radioactivity is accumulated in pro-glacial areas, and pose a risk of potential ecological impacts (Łokas et al., 2014,2017,2019; Owens et al., 2019).

In this study we present data concerning cryoconite collected at the Morteratsch glacier, in the Swiss Alps. We aim to understand whether cryoconite radioactivity is uniform across the surface of glaciers, or if it is influenced by local factors, such as the position of cryoconite deposits on the ice surface, the connection with the supraglacial hydrological system, and its aggregation state. It is well known that the supraglacial environment is highly dynamic, in particular when considering the lower sectors of glaciers, where ice melt and motion, liquid precipitation, and meltwater runoff continuously shape the glacial surface (Rippin et al., 2015; Rossini et al., 2018). The effects of these processes on cryoconite are manifold, affecting the morphology and distribution of its deposits (Cook et al., 2016; Takeuchi et al., 2018), its biological communities (Pittino et al., 2018; Zawierucha et al., 2019) and its biogeochemical composition (Bagshaw et al., 2007). Improved knowledge on these processes is necessary to better understand how the transience of the supraglacial environment influences the radioactive content of cryoconite, and if the latter can be used as a tracer to provide insight into the dynamics of supraglacial hydrology.

2. Study site and sampling

Cryoconite was sampled at the Vadret da Morteratsch glacier on July 18th 2018. The glacier is the largest in the Bernina range (Rhaetian Alps, Switzerland, see Fig. 1). It is a north-facing valley glacier whose basin extends from 2100 to 4049 m a.s.l.. The glacier is experiencing a rapid retreat as a consequence of a strong imbalance between its geometry and contemporary climate. Retreat and thinning are contributing to a significant darkening of the ice surface in the lower sectors of the glacier, with the emergence of sub glacial debris (Rossini et al., 2018) and the deposition of mineral dust from the surrounding moraines (Oerlemans et al., 2009). This environment is favorable for the formation of cryoconite, which has previously been investigated at this site in relation to the effects on the optical properties of ice (Di Mauro et al., 2017) and to its ability to accumulate radioactivity

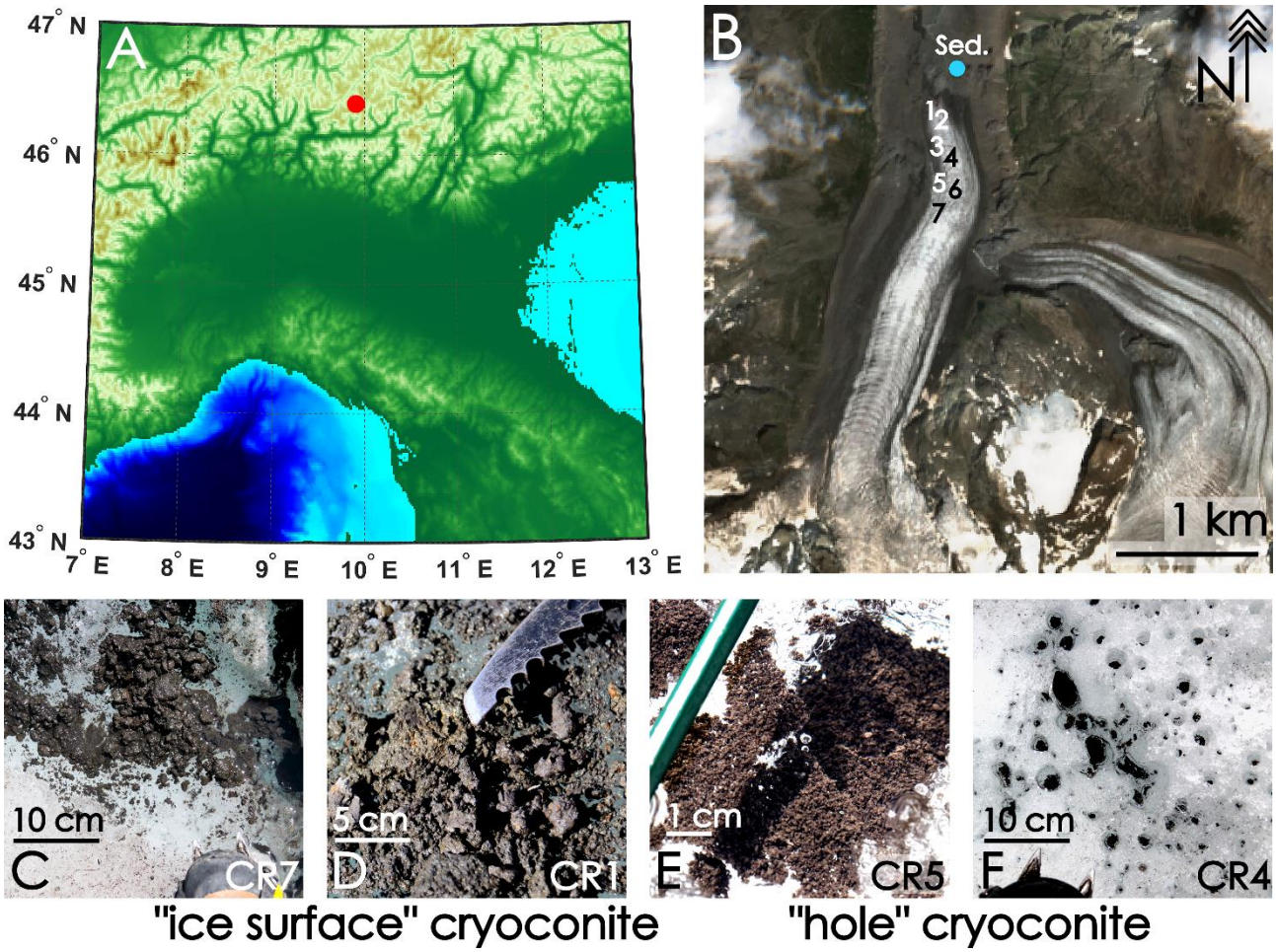

Fig. 1 The geographic setting of the present study. The relief map (panel A) shows the position of Vadret da Morteratsch within the Alps (red dot). In panel B a satellite picture of the glacier is presented (Sentinel 2, ESA), retrieved on July 16th, 2018. Sampling sites are highlighted by numbers corresponding to cryoconite sample codes, and by a blue dot (riverine proglacial sediments). In the lower row, examples of cryoconite samples belonging to the "ice surface" (C,D) and "hole" (E,F) types are shown.

and heavy metals (Baccolo et al., 2017). The sampling campaign of July 2018 was carried out to continue monitoring activities established in 2015. Attention was paid to the morphological features of cryoconite and to its proximity to supraglacial hydrology. It was noted during previous campaigns that cryoconite deposits at Vadret da Morteratsch can be distinguished in two types, namely "hole" and "ice surface" deposits. Cryoconite accumulated in deposits defined as "hole", is found at the bottom of holes melted into ice which are filled with meltwater. The diameter of ice holes is variable, ranging from less than 1 cm to tens of cms. "Ice surface" cryoconite is accumulated in thick and massive deposits only poorly connected with meltwater. During our expeditions, we have always found both cryoconite types, but "hole" deposits are more common at the beginning of the melt season and at high elevation, while "ice surface" deposits are more commonly found in the lower sectors of the glacier and at the end of the melt season.

Since the main objective of our work is to understand if the radioactivity content of cryoconite is somehow influenced by cryoconite morphology and supraglacial processes, we planned the campaign for late July, in the middle of the melt season, so as to optimize the chances of finding both "hole" and "ice surface" deposits. We collected three cryoconite samples from deposits

corresponding to "hole" features, three from "ice surface" deposits and one from a deposit showing "intermediate" characteristics. The elevation of cryoconite sampling sites ranged from 2100 to 2300 m a.s.l.. In addition, sediments have been collected near the terminus at a small proglacial river. All the collected samples have been considered to the aims of this study and no selection has been carried out. Example pictures of cryoconite types are shown in Fig. 1, while extensive descriptions and photographs of our sampling sites/types are found in the Supplementary Material.

Sample collection was conducted with clean plastic spatulas and disposable pipettes, and samples were stored in sterile plastic tubes. Cryoconite deposits with abundant material were chosen during the field campaign, so as to obtain large samples and facilitate subsequent analyses. After the collection, samples were kept at 0°C in a thermal bag during the campaign and subsequently stored at -20°C in the Eurocold Laboratory of the Milano-Bicocca University, until the preparation for the analyses.

3. Materials and methods

The radioactivity of cryoconite in our samples has been investigated through γ-spectrometry. Samples were dried until a constant weight at about 60°C. Coarser fragments were manually removed. Cryoconite was then stored in clean polyethylene Petri dishes (diameter 9.0 cm, height 1.5 cm) and sealed in plastic bags to prevent radon loss. Sample mass varied between 4 and 77 g depending on availability. Dishes were chosen to increase the surface area to volume ratio of samples, so as to limit radiation self-absorption and improve the analytical efficiency. Counting took place some months after sealing the samples, when the secular equilibrium between ^{222}Rn and its progenies was reached. A Broad Energy High Purity Germanium detector was used for the acquisition of the spectra. The detector registers an energy spectrum from 3 to 3,000 keV, with the following energy resolution: 0.5 keV at 59.5 keV, 1.2 keV at 661 keV and 1.6 keV at 1,332 keV (intended as full width half maximum resolution). The detector is provided with a germanium crystal (relative efficiency 50 %) whose active volume is 150 cm^3. Each sample was counted for a variable time ranging from 7 to 14 days in relation to its mass. After the acquisition, spectra were processed for peak identification and fitting and the absolute detection efficiency was calculated via Monte Carlo simulations (Baccolo et al., 2017). If possible, for each nuclide two γ-energies were considered for the analysis. No corrections related to spectral interferences were required with the exception of ^{226}Ra, as its main γ-ray (186.2 keV) overlapped that of ^{235}U at 185.7 keV. To disentangle the two contributions an additional γ-line (163.4 keV) from ^{235}U was considered. A blank spectrum was acquired by counting an empty Petri dish for 10 days. Traces of ^{214}Pb (22 ± 3 mBq), ^{214}Bi (20 ± 5 mBq) and ^{40}K (80 ± 3 mBq) were detected and subtracted from the sample signals. The blank contribution of ^{214}Pb and ^{214}Bi represents 1 % of the signal detected in the samples, while for ^{40}K the value is 0.3 %. Minimum detectable activities (MDA) have been calculated considering the background integral counts below the peaks associated to the γ-energies of interest. They range from 0.1 Bq kg^{-1} for ^{137}Cs to 22 Bq kg^{-1} for ^{230}Th. Full details concerning analytical performance are reported in the Supplementary Material.

Most of the detected radionuclides belong to the ^{238}U (^{234}Th, ^{234m}Pa, ^{230}Th, ^{226}Ra, ^{214}Pb, ^{214}Bi, ^{210}Pb), ^{235}U (^{235}U, ^{227}Th) and ^{232}Th (^{228}Ac, ^{224}Ra, ^{212}Pb, ^{212}Bi, ^{208}Tl) decay chains. Other observed nuclides are cosmogenic (^{7}Be), primordial (^{40}K) or artificial (^{108m}Ag, ^{137}Cs, ^{207}Bi, ^{241}Am). Activity concentrations of ^{7}Be, ^{108m}Ag, ^{137}Cs, ^{207}Bi, ^{210}Pb$_{exc.}$ and ^{241}Am have been corrected for decay to the sampling date.

Mean activities of ^{214}Pb and ^{214}Bi have been used to distinguish the atmospheric (excess or unsupported) and lithogenic (supported) fractions of ^{210}Pb.

The carbonaceous content of samples was also analyzed. Elemental and organic carbon (EC and OC respectively) were quantified through a thermo-optical method. A Sunset EC/OC analyzer (Sunset Lab Inc.) was used, following the NIOSH 5040 protocol (Birch and Cary, 1996). Samples were suspended on quartz fiber filters (Pall, 2500QAO-UP, 47 mm diameter), after pre-firing at 700°C for 1 hour to remove contaminations. Filters were weighed before and after deposition in a conditioned room (T = 20 ± 1 °C, rel. um. = 50 ± 5 %). The amount of cryoconite deposited on each filter was determined with an analytical microbalance (precision = 1µg) operated in the conditioned room. Electrostatic interferences were prevented through a deionizing gun. EC and OC mass concentration were inferred from the mass of cryoconite deposited on filters and the EC-OC surface concentration. OC was converted into organic matter (OM), following the convention by Pribyl (2010).

4. Results

4.1. Analytical performance

With respect to previous radiological measurements in cryoconite, this work represents a step toward increased analytical performances. The use of a customized Broad Energy HP-Ge detector in place of a commercial well HP-Ge detector and the analysis of massive cryoconite samples contributed to the improved results presented here. Considering our previous work as a benchmark (Baccolo et al., 2017), analytical sensitivity has been increased on average by a factor of 8.4, with several MDA less than 1 Bq kg^{-1}. With respect to other studies concerning the characterization of sediments and soils, MDAs presented here (Supplementary Material) are one order of magnitude lower (Malain et al., 2012). This improvement can be attributed to the better shielding from background radioactivity, higher mass of the samples, increased energy resolution and detector efficiency. Thanks to the increased sensitivity, we have expanded the number of detected radionuclides, now including nuclides of the ^{235}U decay chain, ^{7}Be (cosmogenic), others belonging to the ^{238}U chain and ^{108m}Ag (artificial). The identification of ^{108m}Ag is an important finding, since this artificial radioactive nuclide ($t_{1/2}$ 418 yr) has never been reported in terrestrial environments. It has only been occasionally observed in tissues of marine organisms where silver is bio-accumulated (Morita et al., 2010), in marine sediments collected at nuclear testing sites in the Pacific (Beasley and Held, 1971), and during the evaluation of material radiopurity for rare event physics experiments (Laubenstein, 2017).

4.2. Radioactive content of cryoconite samples

4.2.1. Natural Radionuclides

The activity of natural radionuclides detected in cryoconite samples is shown in Fig. 2. It can be seen that in dealing with lithogenic nuclides, the radioactivity is comparable to the values characterizing the upper continental crust (UCC) reference, particularly for ^{40}K and ^{232}Th-related nuclides. For ^{238}U-progenies, an activity slightly higher than UCC is noted. The UCC reference for ^{235}U and ^{238}U is 1.55 and 33.8 Bq kg^{-1} respectively, while on average cryoconite samples present an activity of 55(13) Bq kg^{-1} (standard deviation) for ^{238}U-chain nuclides (without considering ^{210}Pb) and of 3.3(1.5) Bq kg^{-1} for ^{235}U. The enrichment is uniform among cryoconite samples from the Morteratsch glacier, and no significant differences are noted when comparing cryoconite types considered here. By

comparing the activity of ^{235}U and ^{234m}Pa, a reference for ^{238}U activity, it is possible to understand if the uranium radioactivity excess depends on a non-lithogenic uranium fraction. Natural uranium has a regular $^{238}U/^{235}U$ activity ratio of 21.7 (Salama et al., 2019); our samples display an average ratio of 21.8, in agreement with the natural value. The result rules out the presence in cryoconite of a uranium fraction whose isotopic composition has been artificially altered (depletion or enrichment for military and commercial purposes). In addition, proglacial sediments collected near the glacier show an enrichment of U- related nuclides, with an activity for the 235- and 238-chains of 3.1(0.3) and 62(9) Bq kg^{-1} respectively, comparable to what is observed in cryoconite. This confirms that the enrichment is specific to the Morteratsch glacial basin. This observation is probably related to uraniferous minerals in the rocks surrounding the glacier, as has also suggested by studies about mineral waters (Stalder et al., 2012).

With respect to the lithogenic radionuclides, $^{210}Pb_{exc.}$ ($t_{1/2}$ 22.3 yr) and ^{7}Be ($t_{1/2}$ 53.1 d) have notable differences. Firstly, they are not directly derived from the radioactive decay of crustal material, since they are natural FRN, as $^{210}Pb_{exc.}$ (excess ^{210}Pb) is the decay product of ^{222}Rn escaped into the atmosphere from the Earth crust, and ^{7}Be is a cosmogenic nuclide produced in the high atmosphere. Their activity in cryoconite is above typical environmental values. In soils and sediments $^{210}Pb_{exc.}$ usually doesn't exceed tens or a few hundred Bq kg^{-1} (Persson and Holm, 2011), while for ^{7}Be typical values in surficial samples are in the range of 10-50 Bq kg^{-1} (Blake et al., 1999; Mabit et al., 2008). The mean activity in cryoconite from the Morteratsch glacier is 1,700(500) and 820(760) Bq kg^{-1} respectively. Unlike uranium, in this case the anomaly concerns the cryoconite only, rather than being characteristic of the catchment since proglacial sediments have an activity compatible with ordinary environmental values: 43(13) Bq kg^{-1} for ^{7}Be, while the activity of $^{210}Pb_{exc.}$ is below MDA (2 Bq kg^{-1}). In addition, significant differences are found between cryoconite types, in particular considering ^{7}Be. For this nuclide the average activity in "ice surface" cryoconite is 34(14) Bq kg^{-1}, in "intermediate" cryoconite it 1,261(111) Bq kg^{-1} and in "hole" cryoconite is 1,473(301) Bq kg^{-1}. For $^{210}Pb_{exc.}$ the higher activity is observed in "intermediate" samples, with a value of 2,550(202) Bq kg^{-1}, while "ice surface" and "hole" samples show similar activities: 1,550 and 1,530 Bq kg^{-1}.

4.2.2. Anthropogenic Radionuclides

The results of this study confirm those of a previous work (Baccolo et al., 2017), demonstrating that cryoconite from the Morteratsch glacier is contaminated with artificial FRN. Results concerning analysis of artificial FRN are presented in Fig. 3 and Tab. 1, and the following radionuclides have been identified in our samples: ^{108m}Ag, ^{137}Cs, ^{207}Bi and ^{241}Am. The identification of ^{108m}Ag ($t_{1/2}$ 418 yr) is particularly relevant, since this is the first finding of ^{108m}Ag in terrestrial environments. It was produced from nuclear reactions involving silver components during test explosions in the 1960s(Grismore et al., 1972). This radionuclide has been detected in three samples, one per cryoconite type. Activity concentrations of ^{108m}Ag in cryoconite are low, ranging from 0.26±0.10 to 0.77±0.37 Bq kg-1 (MDA: 0.24 Bq kg-1). It has not been observed in proglacial sediments. The identification of(Grismore et al., 1972). This radionuclide has been detected in three samples, one per cryoconite type. Activity concentrations of ^{108m}Ag in c ryoconite are low, ranging from 0.26±0.10 to 0.77±0.37 Bq kg^{-1} (MDA: 0.24 Bq kg^{-1}). It has not been observed in proglacial sediments. The identification of ^{207}Bi ($t_{1/2}$ 31.5 yr) in the environment is also rather rare, although it has been previously detected in some terrestrial environments (Bossew et al., 2006) and in cryoconite (Tieber et al., 2009; Baccolo et al., 2017, 2019). Its production in the Northern Hemisphere is associated

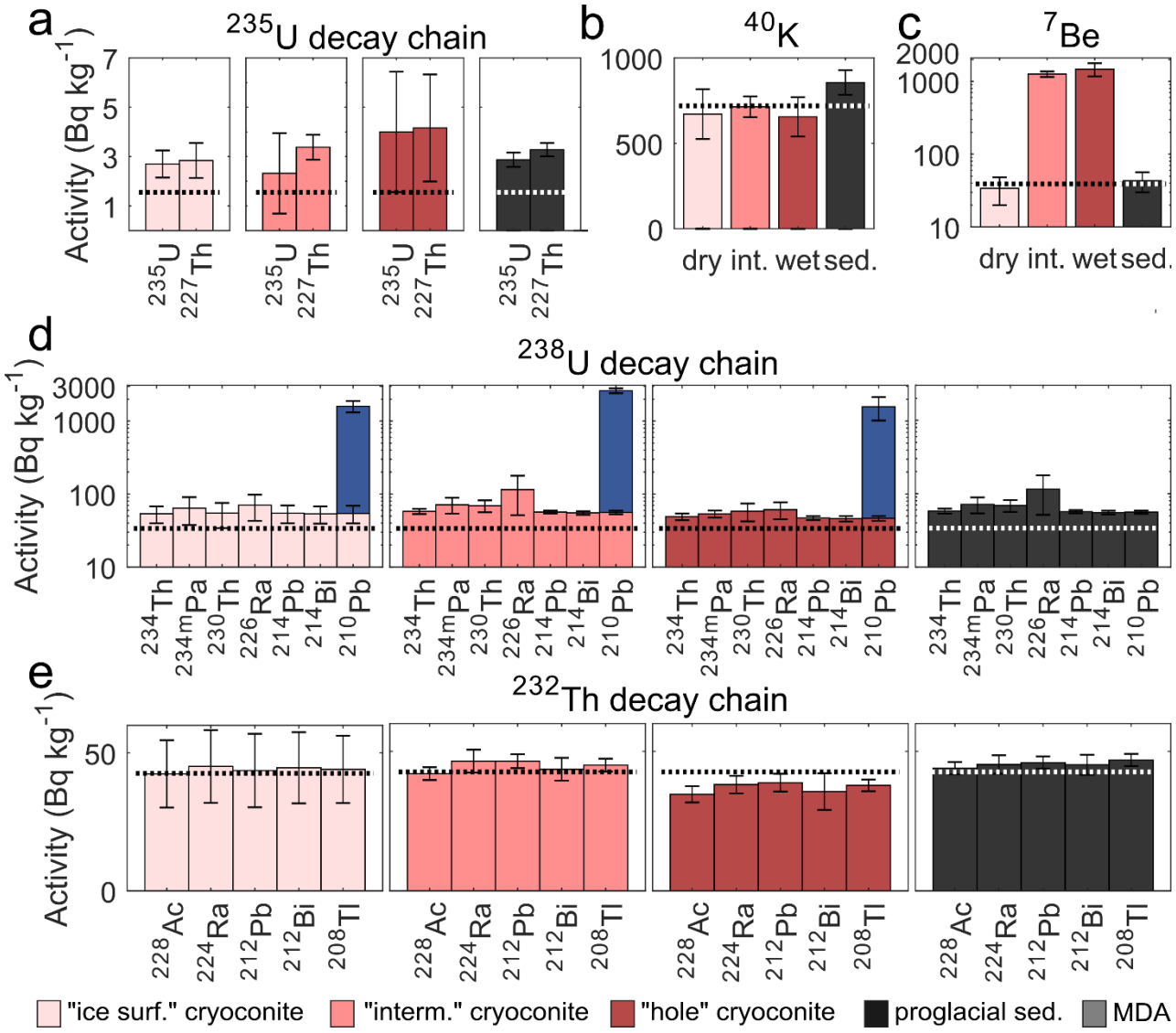

Fig. 2 Natural radionuclides in cryoconite samples from the Morteratsch glacier. Data refer to "ice surface", "intermediate" and "hole" cryoconite types, and to proglacial sediments (sed.) collected near the glacier terminus. The dashed line corresponds to average UCC activities, calculated from the reference by Rudnick and Gao (2003). The reference for ^{7}Be is taken from Blake et al. (1999) and Mabit et al. (2008). ^{210}Pb activity is represented for both supported (red shades) and excess fractions (blue).

with the explosion of the Tzar thermonuclear device in 1961 in Novaja Zemlja (Bossew et al., 2006). ^{207}Bi was found in six of the seven cryoconite samples presented in this study. On average its activity in "ice surface" cryoconite is 2.8(3.1) Bq kg^{-1}, in "intermediate" cryoconite is 1.4(0.3) Bq kg^{-1} and in "hole" cryoconite is 0.5(0.2) Bq kg^{-1}. In proglacial sediments its activity is lower than MDA, (0.3 Bq kg^{-1}). We found similar results for ^{241}Am ($t_{1/2}$ 432.2 yr), where the highest concentrations are found in "ice surface" cryoconite with an average activity of 17(20) Bq kg^{-1}. Lower activities characterize "intermediate" and "hole" samples for ^{241}Am, with mean values of 8.7(0.6) and 1.5(1.4) Bq kg^{-1} respectively. In proglacial sediments the activity is lower than MDA (0.2 Bq kg^{-1}). Despite being considered a relatively rare artificial radionuclide, ^{241}Am has been reported several times in the environment though at lower concentrations in comparison to the results presented here (Shabana and Al-Shammari, 2001). Its occurrence is mostly related to nuclear test explosions and its

Tab. 1 Average activity data for the four sample types considered here: ""ice surface"", "hole" and "intermediate" cryoconite, and proglacial sediments.

	analyte	"ice surf." cryoconite (n=3)	"intermediate" cryoconite (n=1)	"hole" cryoconite (n=3)	proglacial sediments (n=1)
^{235}U chain *(Bq kg^{-1})*	**^{235}U**	2.7±0.5	2±2	4±2	2.9±0.3
	^{227}Th	2.8±0.7	3.4±0.5	4±2	3.3±0.3
^{238}U chain *(Bq kg^{-1})*	**^{234}Th**	54±14	58±5	49±5	54±4
	^{234m}Pa	64±27	54±6	71±18	70±16
	^{230}Th	55±21	69±13	58±16	58±11
	^{226}Ra	71±28	115±64	61±16	78±15
	^{214}Pb	55±15	57±3	47±3	57±3
	^{214}Bi	54±14	55±3	46±4	57±3
	^{210}Pb$_{tot}$	1,604±285	2606±199	1577±557	1,684±132
	^{210}Pb$_{supp}$	54±15	56±3	47±4	57±3
	^{210}Pb$_{exc}$	1,550±271	2,550±202	1,530±557	< 2
^{232}Th chain *(Bq kg^{-1})*	**^{228}Ac**	42±12	42±2	35±3	44±2
	^{224}Ra	45±13	47±4	38±3	45±3
	^{212}Pb	44±13	47±3	39±3	46±2
	^{212}Bi	45±13	44±4	36±7	45±4
	^{208}Tl	44±12	45±2	38±2	47±2
single nuclides *(Bq kg^{-1})*	**^{7}Be**	34±14	1,261±111	1,473±301	43±13
	^{40}K	671±14	714±61	655±115	856±72
	^{108m}Ag	0.3±0.1	0.3±0.1	0.4±0.3	< 0.2
	^{137}Cs	1,369±1,455	628±40	150±97	0.89±0.09
	^{207}Bi	3±3	0.5±0.2	1.4±0.3	< 0.3
	^{241}Am	17±20	9±1	1±1	< 0.2

(*continued*)

	analyte	"ice surf." cryoconite (n=3)	"intermediate" cryoconite (n=1)	"hole" cryoconite (n=3)	proglacial sediments (n=1)
carbonaceous content *(% m/m)*	**organic carbon**	3±1	3.6±0.2	4±1	0.45±0.02
	elemental carbon	0.6±0.4	0.34±0.02	0.2±0.1	< 0.01
	organic matter	6±2	7.2±0.4	8±2	0.90±0.04

290 environmental activity is increasing, owing the decay of its parent nuclide ^{241}Pu (Thakur and Ward, 2018). The distribution of ^{137}Cs in cryoconite resembles those of ^{207}Bi and ^{241}Am, with the highest activity being found in "ice surface" cryoconite, with a mean value exceeding 1,000 Bq kg^{-1}. In "intermediate" and "hole" samples the activity is lower: 628(40) and 150(97) Bq kg^{-1} respectively.

4.3. Carbonaceous content

295 The variability of OM content in cryoconite samples is high, as is depicted in Fig. 3e, where it is evident that the concentration of OM is more variable within single cryoconite types than when comparing the different types with each other. The average values for each cryoconite type is similar, with a mean concentration (% mass fraction) in "ice surface" cryoconite of 3(1) %, in

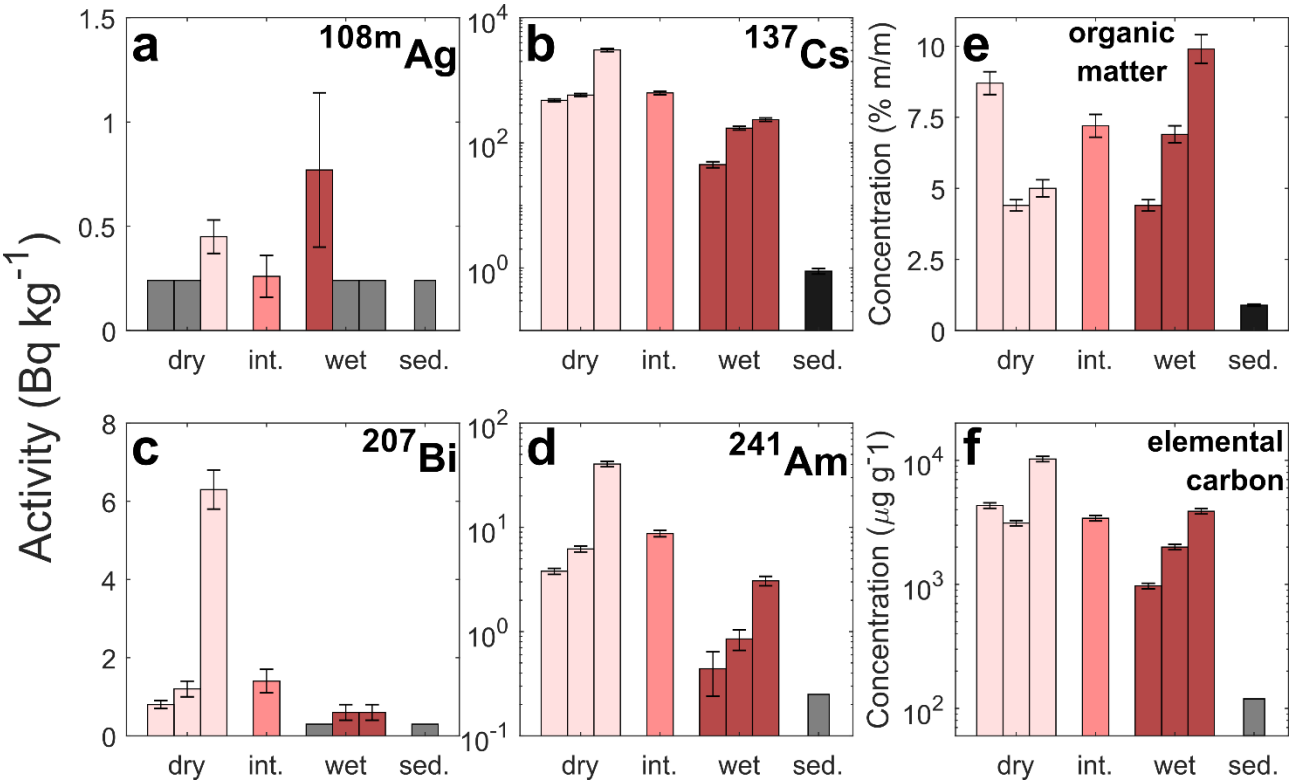

300 **Fig. 3 Concentration activity of artificial radionuclides detected in cryoconite from the Morteratsch glacier (a-d) and carbonaceous fractions (e-f). Data are grouped based on the three cryoconite types; red bars represent single samples, and grey bars MDA values.**

"intermediate" and "hole" cryoconite of 3.6(0.2) and 4(1) % respectively. The OM fraction in proglacial sediments is limited, representing only 0.45(0.02) % of total mass. Results of analysis for EC (Fig. 3f) are similar to those concerning ^{137}Cs, ^{207}Bi and ^{241}Am, that is, the highest concentrations are found in "ice surface" cryoconite, with a mean mass fraction of 0.59(0.38) % and the lowest in "hole" cryoconite, with a mean value of 0.23(0.15) %. "Intermediate" cryoconite has a concentration of 0.34(0.02) %. In proglacial sediments the concentration of EC is lower than MDA (0.01 %).

5. Discussion

5.1. Correlation analysis

To explore the relationships between radionuclides and impurities analyzed in cryoconite, a combination of Pearson's correlation coefficients and cluster analysis was applied (Fig. 4a). To obtain robust results, ^{235}U, ^{234m}Pa, ^{226}Ra and ^{108m}Ag were not considered, owing the high relative errors associated with these variables (larger than 30%). Three clusters in the data are identified. The largest cluster includes the natural lithogenic radionuclides, highlighting that these nuclides correlate with each other, as they are associated with the mineral fraction of cryoconite. An example of the high correlation within this cluster is depicted in Fig. 4b, where the activity of ^{214}Pb (belonging to the ^{238}U-chain) is compared to ^{208}Tl (belonging to the ^{232}Th-chain). A second cluster is defined by artificial FRN and EC, i.e. the anthropogenic species detected in cryoconite. The correlation between the variables of this cluster is notable, with coefficients exceeding 0.9 (see also Fig. 4c). This suggests that both FRN and EC display an affinity for cryoconite and likely for its OM fraction. It is well-known that many radionuclides have an affinity for OM (Livens and Baxter, 1988; Chuang et al., 2015), which is abundant in cryoconite, while the relationship between OM and EC remains poorly investigated. In addition, the positive correlation coefficients characterizing this cluster are indicative of the common source of the anthropogenic species found in cryoconite, the atmosphere. In fact, the only possible source for both EC and anthropogenic radionuclides in glacial environments is the atmosphere, and specifically atmospheric deposition. The third cluster is defined by ^{7}Be, ^{210}Pb$_{exc.}$ and OM. The correlation coefficients within this cluster are lower and range from 0.5 to 0.7 (see also Fig. 4d), however the correlation between these variables confirms that OM in cryoconite plays an important role in the accumulation of atmospheric fallout and pollutants, as previously described for other contexts (Gadd, 1996; Accardi-Dey and Gschwend, 2002; Chuang et al., 2015).

Also visible in the correlation matrix is the negative correlation between ^{40}K and OM. This is possibly related to the fact that as cryoconite is composed of both mineral and organic fractions of different proportions, the higher is one of the two and the lower is the other one. In fact, organic matter is not only negatively correlated with ^{40}K, but with all the lithogenic radionuclides. Another observation from the matrix concerns ^{7}Be. This is negatively correlated with artificial species and with many of the lithogenic nuclides. The negative correlation with lithogenic nuclides is likely related to its positive correlation with OM, which is in turn negatively correlated with lithogenic nuclides. The negative correlation between ^{7}Be and the anthropogenic species is more difficult to interpret, since both share an atmospheric origin and are deposited on the glacier in association with precipitation. What sets them apart, however, is their residence time on glaciers. Artificial FRN considered here have half-lives of decades or more, and EC is a stable compound, particularly in the cold environments associated with glacial settings (Cheng et al., 2008). Conversely, ^{7}Be has a short half-life (53 d) and its presence within cryoconite is likely controlled by different processes.

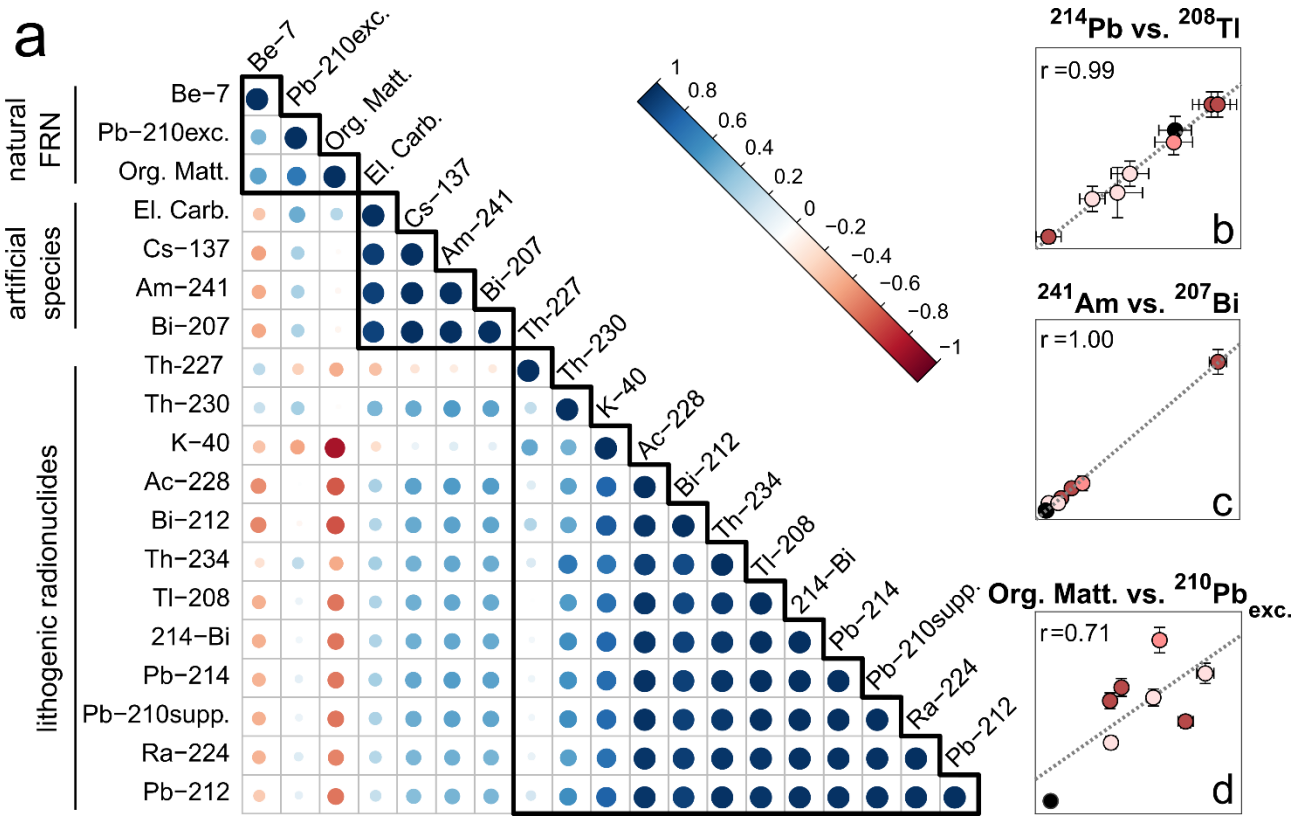

Fig. 4 Correlation among the variables considered in this study. In panel a the correlation is illustrated using a Pearson's correlation matrix where correlation coefficients are represented by circles whose color and size depend on their value. Variables have been ordered and clustered into three groups, following a hierarchical clustering approach. Clusters are defined by black solid lines. Panel b-d: linear correlation between selected variables belonging to the three clusters; the same color palette of Fig. 2 has been used.

5.2. Radioactivity content in different cryoconite types

The cryoconite types explored in this study show differences in terms of radioactivity and carbonaceous content (Fig. 2, Fig. 4 and Tab. 1). In "ice surface" cryoconite artificial FRN are abundant, while "hole" samples are rich in ^{7}Be. To investigate if such differences are relevant, a Student's t test (significant at 5%) was applied. Considering the "ice surface-intermediate", "ice surface-hole" and "intermediate-hole" pairs, we have selected only the variables showing a statistically significant difference with respect to two or three pairs. $^{210}Pb_{exc.}$, ^{137}Cs, ^{7}Be and OM satisfy this condition. To understand which variables contribute most to variance between different cryoconite types, multiple linear regression has been applied to model the relationship between the variables and the cryoconite type ("ice surface", "intermediate" or "hole"). The complete model taking into account all four variables, has relatively good performances (R-squared = 0.73, Supplementary Material). To determine which of the variables contributes most, four additional models have been calculated in which single variables have been excluded one at a time (Supplementary Material). The variable whose absence determines the largest decrease in classification performance is ^{7}Be, which is responsible for more than 85% of the variance explained in the complete model. In fact, the model calculated excluding ^{7}Be has an R-squared value lower than 0.1. ^{7}Be is the most discriminating variable being abundant in "hole" cryoconite, scarce in "ice surface" samples and showing intermediate activity concentrations in "intermediate" samples (Fig.

2c). The only other variable which contributes substantially to the model is OM, which accounts for 8 % of the variance explained in the complete model. The variability of OM in cryoconite resembles that of ^{7}Be: higher concentrations in "hole" samples, lower ones in "ice surface" samples.

5.3. Understanding cryoconite radioactivity in relation to the supraglacial environment

It has been demonstrated that the composition of cryoconite from the Morteratsch glacier is far from uniform. To begin to understand the processes involved in creating these differences, the features characterizing cryoconite types must be considered. "Hole" cryoconite deposits display small defined granules (1-2 mm) and are always in contact with meltwater (see the Supplementary Material). In fact, cryoconite sediment characterizing "hole" deposits is found at the bottom of small cavities deepened into ice and filled with meltwater which is continuously supplied by active meltwater channels. On the contrary, "ice surface" cryoconite is accumulated in thick and dry deposits not in contact with meltwater, being usually found in areas of the glacier rich in ice cracks and crevasses which locally drain surficial channels. In addition, "ice surface" cryoconite doesn't present granules, being the sediment more massive and not showing aggregation patterns.

The concentration of ^{7}Be in cryoconite, which ranges from 34 Bq kg^{-1} in "ice surface" cryoconite to 1,473 Bq kg^{-1} in "hole" cryoconite, can be explained considering the different degree of connection with supraglacial hydrology. On glaciers, the sources of ^{7}Be are snow and rain, where it accumulates through scavenging in association with aerosol (Ioannidou et al., 2005). Due to its relatively short half-life (53 d), this radionuclide is typically found in recently deposited and shallow snow, and is less likely to be present in older, deeper snow and ice. The process most likely responsible for rapid mobilization of ^{7}Be on the surface of glaciers is supraglacial runoff induced by the melt of recent snow (Smith et al., 2000). "Hole" cryoconite is in contact with active supraglacial channels, it therefore interacts with meltwater and accumulates ^{7}Be. The presence of OM and extra-cellular polymeric substances, which are both affine for radionuclides (Gadd, 1996; Chuang et al., 2015), likely favors the accumulation.

The activity of ^{7}Be in "ice surface" samples is similar to that which was measured in proglacial sediments (34 vs. 43 Bq kg^{-1}). These values are comparable with those observed in soils and sediments where ^{7}Be is present because of direct atmospheric deposition, without the involvement of accumulation processes (Blake et al., 1999; Mabit et al., 2008). The scarcity of ^{7}Be in "ice surface" cryoconite suggests a limited interaction between these deposits and surficial meltwater in the weeks preceding sampling. This agrees with the poor connection with supraglacial hydrology characterizing these samples. But while ^{7}Be is scarce in "ice surface" cryoconite, the opposite is true for artificial FRN and EC, which are more abundant in "ice surface" samples than in "hole" ones (Fig. 3). Considering that the only source of artificial FRN and EC on the surface of glaciers is meltwater (Baccolo et al., 2019), their abundance in "ice surface" cryoconite points to a prolonged interaction time with meltwater, but not in the season when our samples were collected, as revealed by the scarcity of ^{7}Be, rather in the past ones. Contrastingly, for "hole" samples the total interaction time with meltwater has likely been shorter (relatively low artificial FRN content), but more recent (high ^{7}Be activity), suggesting that they have been in contact with meltwater for a longer time in the present melt season compared with "ice surface" samples. "Ice surface" samples described in this study are thus interpreted as samples rich in mature cryoconite which has been accumulated at the

surface of the Morteratsch glacier in previous ablation seasons. Conversely, relatively recent cryoconite, which was still forming when samples were collected, prevails in "hole" samples.

The aggregation state of cryoconite and its OM content agree with the interpretation. "Hole" samples display millimetric aggregates, while "ice surface" samples show no clear aggregation patterns (see Fig. 1 and Supplementary Material). Formation of cryoconite granules has been previously attributed to the interaction between mineral sediments and microbes. Clear aggregation in cryoconite relates to high microbiological activity, while poor or absent aggregation is indicative of limited microbial activity (Takeuchi et al., 2010; Langford et al., 2010). The lack of aggregation in "ice surface" samples and their low OM content, suggest a limited microbiological activity, in accordance with the poor hydrological connection and paucity of liquid water, essential for enabling microbes to flourish on glaciers (Hodson et al., 2010; Langford et al., 2010). "Hole" samples are well connected with meltwater channels and represent an ideal environment for microorganisms, as confirmed by the presence of aggregates and higher OM concentrations. Another factor supporting the interpretation is the variable mass of the cryoconite deposits sampled in this study. "Ice surface" samples are characterized by a notable accumulation of sediments, "hole" ones are more scarce (see photographs in the Supplementary Material). This difference can be related to the degree of maturity of the deposits as well. "Ice surface" deposits, partially consisting in cryoconite formed in previous melt seasons, have had a longer time to develop and accumulate mass. "Hole" deposits are more recent and were still actively forming during filed campaign for this study. The sample identified as "intermediate" displays intermediate features between "ice surface" and "hole" cryoconite types. It has been sampled from a deposit that, despite presenting the typical "hole" features (aggregation and connection with meltwater), was particularly abundant, which is more characteristic of "ice surface" deposits. From a radiological point of view, "intermediate" cryoconite is rich in ^{7}Be, artificial FRN and EC, suggesting both recent and past interactions with meltwater. These features could be explained as follows: the "intermediate" sample consists in a deposit where cryoconite from past seasons has been reactivated in response to a renewed connection with meltwater during the 2018 ablation season.

6. Conclusions

Analysis of cryoconite from the Morteratsch glacier further supports previous results suggesting that cryoconite has an extraordinary ability to accumulate radionuclides. ^{108m}Ag has been detected in three cryoconite samples within this study, representing the first time this artificial radionuclide has been described within terrestrial environments. This result suggests that cryoconite should be considered for future studies concerning the occurrence of rare and poorly investigated radionuclides. But despite the notable radioactive content, the amount and type of radioactivity present in cryoconite collected on Morteratsch glacier are not uniform. Cryoconite from deposits that are in contact with meltwater channels and are characterized by well-defined granules, are extremely rich in short-lived ^{7}Be ($t_{1/2}$ 53.1 d). Deposits that are poorly connected with the supraglacial hydrological system, and that are not characterized by aggregation, are rich in long-lived artificial fallout radionuclides ($t_{1/2}$ > 30 yr) and elemental carbon. The different half-lives of radionuclides have allowed to discuss these differences in relation to the dynamics characterizing the supraglacial hydrological system and to the degree of maturity of cryoconite. A high concentration of ^{7}Be in cryoconite is indicative of a recent interaction with meltwater, while the progressive accumulation of artificial radionuclides can be referred to a prolonged interaction with

meltwater. Focusing on these radiological features, it has been possible to distinguish deposits rich in cryoconite that formed in the previous ablation seasons, from deposits that were likely undergoing active formation while sampling was conducted.

Despite being preliminary and involving a limited number of samples, this study shows that radionuclides, in particular ^{7}Be, can be used as tracers to gather information on the maturity degree of cryoconite and on its age and explore supraglacial dynamics. Further studies are needed to investigate the relationships between the accumulation of radioactivity, organic matter and biological activity of cryoconite. To this aim, it would be desirable to consider different granulometric and compositional fractions of cryoconite and also other environmental samples from the surface of glaciers, such as ice and meltwater.

Acknowledgments

This study has been supported by the Project of Strategic Interest NextData, funded by the Italian National Research Program PNR 2011-2013, and by the project "Impatto degli aerosol e delle polveri fini provenienti dall'area Mediterranea e dal Nord Africa sulla criosfera Alpina", funded by "Dipartimento per gli affari regionali e le autonomie della Presidenza del Consiglio dei Ministri".

References

Accardi-Dey, A.M., Gschwend, P.M. 2002. Assessing the combined roles of natural organic matter and black carbon as sorbents in sediments. Environ. Sci. Technol 36, 21-29.

Appleby, P.G. 2008. Three decades of dating recent sediments by fallout radionuclides: a review. Holocene 18, DOI: 10.1177/0959683607085598.

Baccolo, G., Di Mauro, B., Massabò, D., Clemenza, M., Nastasi, M., Delmonte, B., Prata, M., Prati, P., Previtali, E., Maggi, V. 2017. Cryoconite as a temporary sink for anthropogenic species stored in glaciers. Sci. Rep. 7,DOI: 10.1038/s41598-017-10220-5.

Baccolo, G., Łokas, E., Gaca, P., Massabò, D., Ambrosini, R., Azzoni, R.S., Clason, C., Di Mauro, B., Franzetti, A., Nastasi, M., Prata, M., Prati, P., Previtali, E., Delmonte, B., Maggi, V. 2019. Cryoconite: an efficient accumulator of radioactive fallout in glacial environments. Cryosphere Discussion*,* in discussion.

Bagshaw, E.A., Tranter, M., Fountain, A.G., Welch, K.A., Basagic, H., Berry Lyons, B. 2007. Biogeochemical evolution of cryoconite holes on Canada Glacier, Taylor Valley, Antarctica. Biogeosciences 112, DOI: 10.1029/2007JG000442.

Beasley, T.M.,Held, E.E. 1971. Silver-108m in biota and sediments at Bikini and Eniewtok atolls. Nature 230, 450-451.

Birch, M.E., Cary, R.A. 1996. Elemental carbon-based method for monitoring occupational exposures to particulate diesel exhaust. Aerosol Sci. Tech. 25, 221-241.

Blake, W.H., Walling, D.E., He, Q. 1999. Fallout beryllium-7 as a tracer in soil erosion investigation. Appl. Rad. Isotopes 51, 599-605.

Bogdal, C., Schmid, P., Zennegg, M., Anslemetti, F.S., Scheringer, M., Hungerbühler, K. 2009. Blast from the Past: Melting Glaciers as a Relevant Source for Persistent Organic Pollutants. Environ. Sci. Technol. 43, 8173-8177.

Bossew, P., Lettner, H., Hubmer, A. 2006. A note on ^{207}Bi in environmental samples. J. Environ. Radioactiv. 91, 160-166.

Cheng, C.H., Lehmann, J., Thies, J.E., Burton, S.D. 2008. Stability of black carbon in soils across a climatic gradient. J. Geophys. Res. Biogeo., 113, DOI: 10.1029/2007JG000642.

Chuang, C.Y., Santschi, P.H., Wen, L.S., Guo, L., Xu, C., Zhang, S., Jiang, Y., Ho, Y.F., Schwehr, K.A., Quigg, A., Hung, C.C., Ayranov, M., Schumann, D. 2015. Binding of Th, Pa, Pb, Po and Be radionuclides to marine colloidal macromolecular organic matter. Mar. Chem. 173, 320-329.

Clemenza, M., Cucciati, G., Maggi, V., Pattavina, L., Previtali, E. 2012. Radioactive fallouts as temporal markers for glaciers ice cores dating. Eur. Phys. J. Plus 127, 1-8.

Cook, J.M., Hodson, A.J., Irvine-Fynn, T.D.L. 2016. Supraglacial weathering crust dynamics inferred from cryoconite hole hydrology. Hydrol. Process. 30, DOI: 10.1002/hyp.10602.

Crozaz, G., Picciotto, E., De Breuk, W. 1964. Antarctic snow chronology with Pb210. J. Geophys. Res. 69, 2597-2604.

Di Mauro, B., Baccolo, G., Garzonio, R., Giardino, C., Massabò, D., Piazzalunga, A., Rossini, M., Colombo, R. 2017. Impact of impurities and cryoconite on the optical properties of the Morteratsch glacier (Swiss Alps). Cryosphere 11, DOI: 10.5194/tc-11-2393-2017.

Eichler, A., Schwikowski, M., Gäggeler, H.W., Furrer, V., Synal, H.A., Beer, J., Saurer, M., Funk, M. 2000. Glaciochemical dating of an ice core from upper Grenzgletscher (4200 m a.s.l.). J. Glaciol. 46, 507-515.

Ferrario, C., Pittino, F., Tagliaferri, I., Gandolfi, I., Bestetti, G., Azzoni, R.S., Diolaiuti, G., Franzetti, A., Ambrosini, A., Villa, S. 2017. Bacteria contribute to pesticide degradation in cryoconite holes in an Alpine glacier. Environ. Pollut. 230, 919-926.

Gadd, G.M., 1996. Influence of microorganisms on the environmental fate of radionuclides. Endeavour 20, 150-156.

Gerringa, L.J.A., Alderkamp, A.C., Laan, P., Thuróczy, C.E., De Baar, H.J.W., Mills, M.M., van Dijken, G.L., van Haren, H., Arrigo, K.R. 2012. Iron from melting glaciers fuels the phytoplankton blooms in Amundsen Sea (Southern Ocean): Iron biogeochemistry. Deep-Sea Res. Pt. II 71-76, 16-31.

Grismore, R., Folsom, T.R., Hodge, V.F., Young, D.R. 1972. A study of the radiosilver signature of the 1961-1962 nuclear weapons testing period. T. New York Acad. Sci. 34, 392-415.

Hodson, A., Cameron, K., Bøggild, C., Irvine-Fynn, T., Langford, H., Pearce D., Banwart, S. 2010. The structure, biological activity and biogeochemistry of cryoconite aggregates upon an Arctic valley glacier: Longyearbreen, Svalbard. J. Glaciol. 56, 349-362.

Huang, J., Kang, S., Ma, M., Guo, J., Cong, Z., Dong, Z., Yin, R., Xu, J., Tripathee, L., Ram, K., Wang, F. 2019. Accumulation of Atmospheric Mercury in Glacier Cryoconite over Western China. Environ. Sci. Technol. 53, 6632-6639.

Ioannidou, A., Manolopoulou, M., Papastefanou, C. 2005. Temporal changes of ^{7}Be and ^{210}Pb concentrations in surface air at temperate latitudes (40°N). Appl. Rad. Isotopes 63, 277-284.

Langford, H., Hodson, A., Banwart, S., Bøggild, C. 2010. The microstructure and biogeochemistry of Arctic cryoconite granules. Ann. Glaciol. 51, 87-94.

Laubenstein, M. 2017. Screening of materials with high purity germanium detectors at the Laboratori Nazionali del Gran Sasso. Int. J. Mod. Phys. A 32, DOI: 0.1142/S0217751X17430023.

Li, Q., Kang, S., Wang, N., Li, Y., Li, X., Dong, Z., Chen, P. 2017. Composition and sources of polycyclic aromatic hydrocarbons in cryoconites of the Tibetan Plateau glaciers. Sci. Tot. Environ. 574, 991-999.

Livens, F.R., Baxter, M.S. 1988. Chemical association of artificial radionuclides in Cumbrian soils. J. Environ. Radioactiv. 7, 75-86.

Li, Y., Kang, S., Yan, F., Chen, J., Wang, K., Paudyal, R., Liu, J., Qin, X., Sillanpää, M. 2019. Cryoconite on a glacier on the north-eastern Tibetan plateau: light-absorbing impurities, albedo and enhanced melting. J. Glaciol. 65, 633-644.

Łokas, E., Barmiński, P., Wachniew, P., Mietelski, J.W., Kawiak, T., Środoń, J. 2014. Sources and pathways of artificial radionuclides to soils at a High Arctic site. Environ. Sci. Pollut. R. 21, 12479–12493.

Łokas, E., Zaborska, A., Kolicka, M., Rózycki, M., Zawierucha, K. 2016. Accumulation of atmospheric radionuclides and heavy metals in cryoconite holes on an Arctic glacier. Chemosphere 160, 162-172.

Łokas, E., Wachniew, P., Jodłowski, P. & Gasiorek, M. 2017. Airborne radionuclides in the proglacial environment as indicators of sources and transfers of soil material. J. Environ. Radioactiv. 178-179, 193-202.

Łokas, E., Zaborska, A., Sobota, I., Gaca, P., Milton, J.A., Kocurek, P., Cwanek, A. 2019. Airborne radionuclides and heavy metals in High Arctic terrestrial environment as the indicators of sources and transfers of contamination. Cryosphere 13, DOI: 10.5194/tc-13-2075-2019.

Mabit, L., Benmansour, M., Walling, D.E., 2008. Comparative advantages and limitations of the fallout radionuclides ^{137}Cs, $^{210}Pb_{ex}$ and ^{7}Be for assessing soil erosion and sedimentation. J. Environ. Radioactiv. 99, 1799-1807.

Malain, D. Regan, P.H., Bradley, D.A., Matthews, M., Al-Sulaiti, H.A., Santawamaitre, T. 2012. An evaluation of the natural radioactivity in Andaman beach sand samples of Thailand after the 2004 tsunami. Appl. Radiat. Isotopes 70, 1467-1474.

Morita, T., Ohtsuka, Y., Fujimoto, K., Minamisako, Y., Iida, R., Nakamura, M., Kayama, T. 2010. Concentrations of ^{137}Cs, ^{90}Sr, ^{108m}Ag, $^{239+240}Pu$ and atom ratio of $^{240}Pu/^{239}Pu$ in tanner crabs, Chionoecetes japonicus and Chionoecetes opilio collected around Japan. Mar. Pollut. Bull. 60, 2311-2322.

Nagatsuka, N., Takeuchi, N., Nakano, T., Kokado, E., Li, Z. 2010. Sr, Nd and Pb stable isotopes of surface dust on Ürümqi glacier No. 1 in western China. Ann. Glaciol. 51, 95-105.

Oerlemans, J., Gleisen, R.H., Van Der Broecke, M.R., 2009. Retreating alpine glaciers: increased melt rates due to accumulation of dust (Vadret da Morteratsch, Switzerland). J. Glaciol. 55, 729-736.

Owens, P.N., Blake, W.H., Millward, G.E., 2019. Extreme levels of fallout radionuclides and other contaminants in glacial sediment (cryoconite) and implications for downstream aquatic ecosystems. *Sci. Rep.* 9, DOI: 10.1038/s41598.

Persson, B.R.R., Holm, E. 2011. Polonium-210 and lead-210 in the terrestrial environment: a historical review. J. Environ. Radioactiv. 102, 420-429.

Picciotto, E, Wilgain, S. 1963. Fission products in Antarctic snow, A reference level for measuring accumulation. J. Geophys. Res. 68, 5965-5972.

Pinglot, J.F., Pourchet, M., Lefauconnier, B., Hagen, J.O., Vaikmäe, R., Punning, J.M., Watanabe, O., Takahashi, S., Kameda, T. 1994. Natural and artificial radioactivity in the Svalbard glaciers. J. Environ. Radioactiv. 25, 161-176.

Pittino, F., Maglio, M., Gandolfi, I., Azzoni, R.S., Diolaiuti, G., Ambrosini, R., Franzetti, A. 2018. Bacterial communities of cryoconite holes of a temperate alpine glacier show both seasonal trends and year-to-year variability. Ann. Glaciol. 59 DOI: 10.1017/aog.2018.16.

Preunkert, S., Legrand, M. 2013. Towards a quasi-complete reconstruction of past atmospheric aerosol load and composition (organic and inorganic) over Europe since 1920 inferred from Alpine ice cores. Clim. Past 9, 1403-1416.

Pribyl, D.W. 2010. A critical review of the conventional SOC to SOM conversion factor. Geoderma 156, 75-83.

Rippin, D.M., Pomfret, A., King, N. 2015. High resolution mapping of supra-glacial drainage pathways reveals link between micro-channel drainage density, surface roughness and surface reflectance. Earth Surf. Proc. Land 40, DOI: 10.1002/esp.3719.

Rizzi, C., Finizio, A., Maggi, V., Villa, S. 2019. Spatial-temporal analysis and risk characterization of pesticides in Alpine glacial streams. Environ. Poll. 248, 659-666.

Rossini, M., Di Mauro, B., Garzonio, R., Baccolo, G., Cavallini, G., Mattavelli, M., De Amicis, M., Colombo, R. 2018. Rapid melting dynamics of an alpine glacier with repeated UAV photogrammetry. Geomorphology 304, 159-172.

Salama, E., El-kameesy, S.U., Elrawi, R. 2019. Depleted uranium assessment and natural radioactivity monitoring in North West of Iraq over a decade since the last Gulf War. J. Environ. Radioactiv. 201, 25-31.

Shabana, E.I., Al-Shammari, H.L. 2001. Assessment of the global fallout of plutonium isotopes and americium-241 in the soil of the central region of Saudi Arabia. J. Environ. Radioactiv. 57, 67-74.

Smith, A.M., Fink, D., Child, D., Levchenko, V.A., Morgan, V.I., Curran, M., Etheridge, D.M., Elliott, G. 2000. ^{7}Be and ^{10}Be concentrations in recent firn and ice at Law Dome, Antarctica. Nucl. Instrum. Meth. B 172, 847-855.

Stalder, E., Blanc, A., Haldimann, M., Dudler, V. 2012. Occurrence of uranium in Swiss drinking water. Chemosphere 86, 672-679.

Takeuchi, N. 2002. Optical characteristics of cryoconite (surface dust) on glaciers: the relationship between light absorbency and the property of organic matter contained in the cryoconite. Ann. Glaciol. 34, 409-414.

Takeuchi, N., Nishiyama, H., Li, Z. 2010. Structure and formation process of cryoconite granules on Urumqi glacier No. 1, Tien Shan, China. Ann. Glaciol. 51, 9-14.

Takeuchi, N., Sakaki, R., Uetake, J., Nagatsuka, N., Shimada, R., Niwano, M., Aoki, T. 2018. Temporal variations of cryoconite holes and cryoconite coverage on the ablation ice surface of Qaanaaq Glacier in northwest Greenland. Ann. Glaciol. 59, DOI: 10.1017/aog.2018.19.

Thakur, P., Ward, A.L., 2018. ^{241}Pu in the environment: insight into the understudied isotope of plutonium. J. Radioanal. Nucl. Chem. 317, 757-778.

Tieber, A., Lettner, H., Bossew, P., Hubmer, A., Sattler, B., Hofmann, W. 2009. Accumulation of anthropogenic radionuclides in cryoconites on Alpine glaciers. J. Environ. Radioactiv. 100, 590-598.

Weiland-Bräuer, N., Fischer, M.A., Schramm, K.W., Schmitz, R.A. 2017. Polychlorinated Biphenyl (PCB)-Degrading Potential of Microbes Present in a Cryoconite of Jamtalferner Glacier. Front. Microbiol. 8, DOI: 10.3389/fmicb.2017.01105.

Zawierucha, K. Buda, J., Nawrot, A. 2019. Extreme weather event results in the removal of invertebrates from cryoconite holes on an Arctic valley glacier (Longyearbreen, Svalbard). Ecol. Res. 34, 370-379.

Supplementary Material: "Artificial and natural radionuclides in cryoconite as tracers of supraglacial dynamics"

Giovanni Baccolo[1,2*], Massimiliano Nastasi[2,3], Dario Massabò[4,5], Caroline Clason[6], Biagio Di Mauro[1], Elena Di Stefano[1,2,7], Edyta Łokas[8], Paolo Prati[4,5], Ezio Previtali[2,3], Nozomu Takeuchi[9], Barbara Delmonte[1,2], Valter Maggi[1,2]

1. Environmental and Earth Sciences Department, University of Milano-Bicocca, P.za della Scienza n.1, Milano, 20126, Italy
2. INFN section of Milano-Bicocca, P.za della Scienza n.3, Milano, 20126, Italy
3. Physics Department, University of Milano-Bicocca, P.za della Scienza n.3, Milano, 20126, Italy
4. Physics Department, University of Genova, Genova, 16146, Italy
5. INFN section of Genova, Genova, 16146, Italy
6. School of Geography, Earth and Environmental Sciences, University of Plymouth, Plymouth, PL48AA, UK
7. Department of Physical, Earth and Environmental Sciences, University of Siena, Siena, 53100, Italy
8. Department of Mass Spectrometry, Institute of Nuclear Physics Polish Academy of Sciences, Kraków, 31-342, Poland
9. Department of Earth Sciences, Graduate School of Science, Chiba University, Chiba, Japan

* corresponding author: giovanni.baccolo@unimib.it

Sample	Elevation (m a.s.l.)	Ice tilt (degrees)	Deposit size (cm)	Description
CR-1	2,235	5	120x40	Appearence: **ICE SURFACE** Collected on a flat region of the glacier near the terminus. This is supposedly the material that filled a cryoconite hole where water is now absent. The material is directly exposed to the atmosphere and dry, no granules and no connection to the supra-glacial hydrology are present. The color of cryoconite is dark and poor of rock-fragments. Thickness of the deposit: massive, several cm.
CR-2	2,250	< 5	400x40	Appearance: **HOLE** Collected from the bottom of an ice cavity several meters long (developed along a foliation of ice). The cavity is full of meltwater and connected to supra-glacial channels. Cryoconite shows poorly outlined granules and presents a light brown color. Ice tilt around the cavity is low and hence meltwater flows slowly, favoring the accumulation of cryoconite inside the cavity. Thickness of the deposit: 4-5 mm.
CR-3	2,260	45°	140x30	Appearance: **ICE SURFACE** The cryoconite deposit is settled on a small ice sledge in the middle of a steep slope (45°). It is dry and completely isolated from meltwater channels, dark brown colored. The deposit is granulometrically classed, with coarse rock fragments at the bottom and fine dry material on the top. An evident red streak is present. It is likely Saharan dust previously transported from a melting snow patch located few meters upward along the slope. Probably dusty meltwater from the patch have passed through the cryoconite deposit which have acted as a filter and retained dust. Thickness of the deposit: massive, several cm.
CR-4	2,285	10	several m^2	Appearance: **HOLE** The deposit is newly formed and cryoconite is not accumulated in well-defined holes but is dispersed in many centimetric depressions carved into ice. The deposits are wet and melt-water is slowly passing through them. Cryoconite show evident millimetric granules and a light brown color; thickness of the deposit: 2-3 mm.
CR-5	2,290	10	multiple deposits, average dimension: 20x15	Appearance: **ICE SURFACE** Similar to CR-4, but few meters upward. It consists in several deposits accumulated at the bottom of small ice holes. Meltwater is flowing on them. Cryoconite show evident millimetric granules and a light brown color; thickness of the deposit: 2-3 mm.

(continued)

Sample	Elevation (m a.s.l.)	Ice tilt (degrees)	Deposit size (cm)	Description
CR-6	2,295	5	20x10	Appearance: **INTERMEDIATE** Collected from a single well-defined and rich deposit accumulated at the bottom of an ice hole directly connected to a meltwater channel. Cryoconite presents evident millimetric granules and a light brown color; thickness of the deposit: 1-2 cm.
CR-7	2,305	5	40x3	Appearance: **ICE SURFACE** This is an old and massive deposit which is partially dry and directly exposed to the atmosphere and partially in contact to melt-water. Cryoconite doesn't present granules and is dark brown colored; thickness of the deposit: massive, several cm.
CR-Sed	2,100	-	-	Riverine proglacial sediments collected from a bar at the edge of a pro-glacial river.

Tab. S1 Information about the cryoconite samples considered in this work. Elevation, tilt of the ice in the area around the collection site, deposit size and description are presented for each sample.

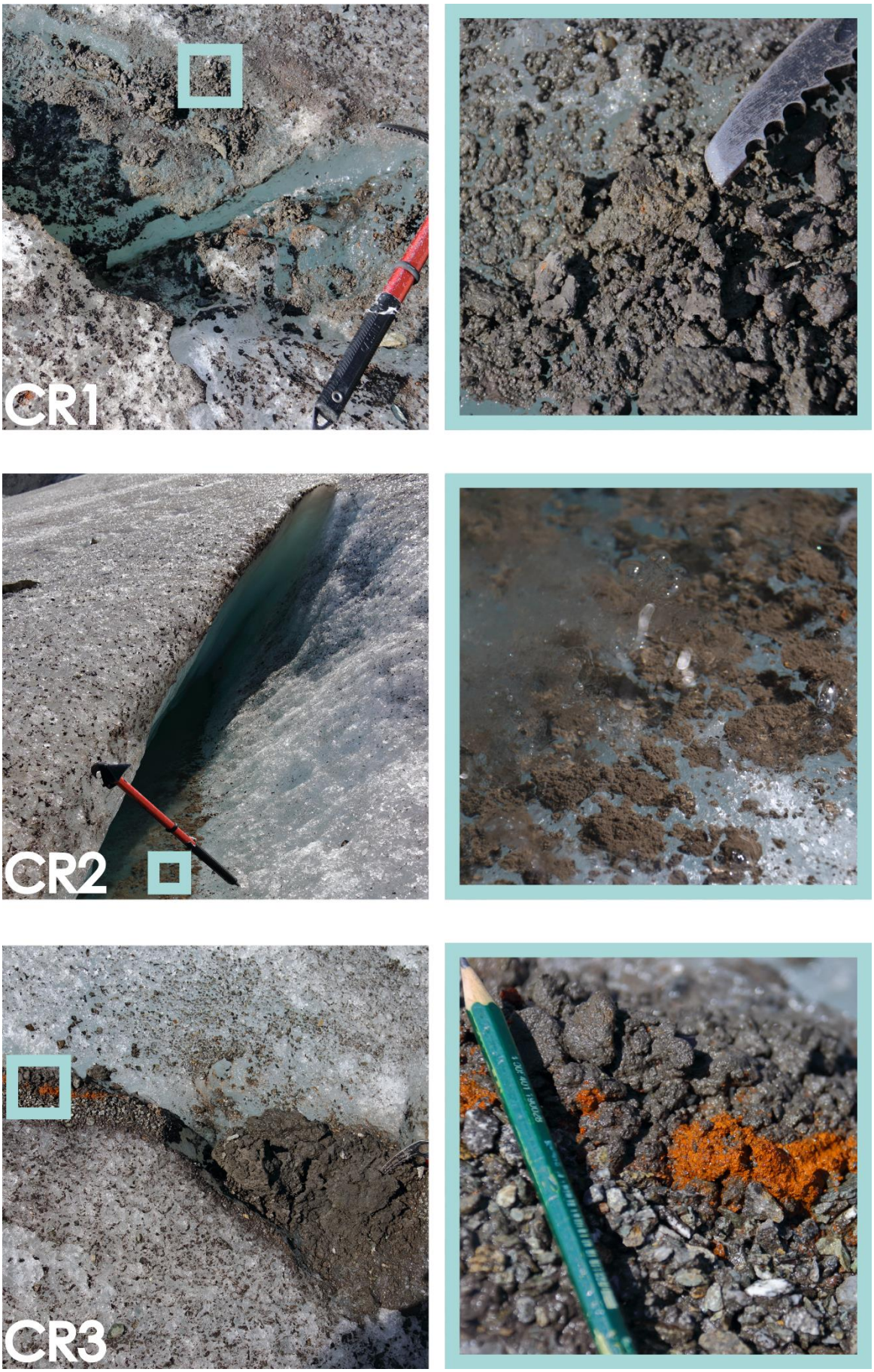

(continued)

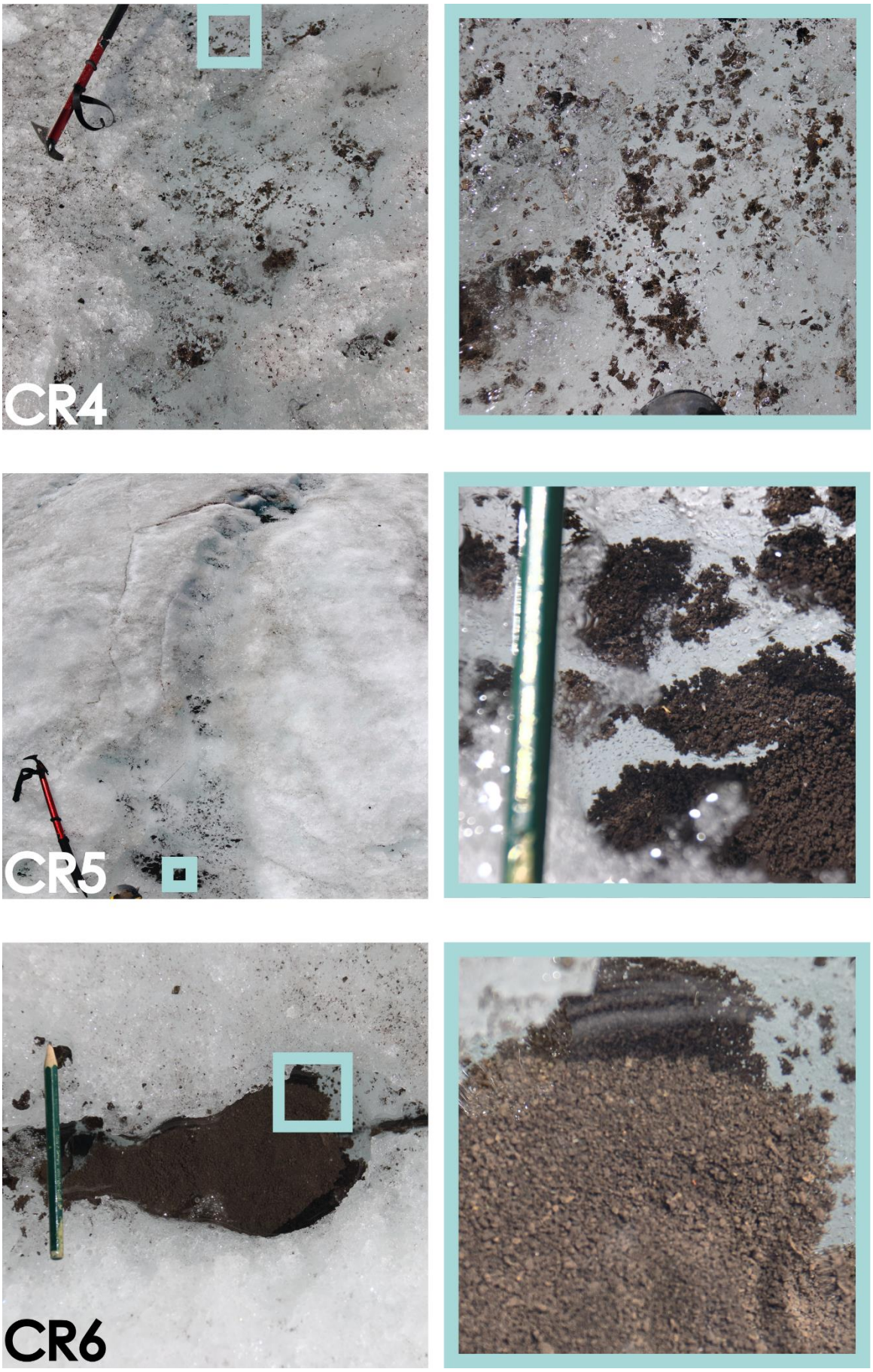

630 *(continued)*

Fig. S1 Pictures of the samples considered in this study. Full descriptions are found in Tab. S1.

Decay Chain	Nuclide	$T_{1/2}$	γ-Energy	Branching Ratio (%)	Detection Absolute Efficiency (‰)	Minimum Detectable Activity (Bq kg^{-1})
^{232}Th	^{208}Tl	183.2 s	583.2	84.5	0.341±0.005	0.6
	^{208}Tl	183.2 s	2614.5	99.0	0.077±0.002	0.5
	^{212}Bi	3633 s	727.3	6.6	0.35±0.01	2.0
	^{212}Bi	3633 s	1620.5	1.5	0.10±0.01	10
	^{212}Pb	10.64 h	238.6	43.3	1.053±0.007	0.3
	^{212}Pb	10.64 h	300.1	3.3	0.67±0.02	5
	^{224}Ra	3.66 d	241.0	4.1	0.99±0.02	3
	^{228}Ac	6.15 h	338.3	11.3	0.79±0.01	1
	^{228}Ac	6.15 h	911.2	25.8	0.26±0.005	0.6
^{235}U	^{227}Th	18.72 d	236.0	12.3	0.82±0.01	1
	^{227}Th	18.72 d	256.2	7.0	0.78±0.02	2
	^{235}U	$7.038\cdot10^{8}$ y	163.4	5.1	1.45±0.03	2
	^{235}U	$7.038\cdot10^{8}$ y	205.3	5.0	1.27±0.02	2
^{238}U	^{210}Pb	22.3 y	46.5	4.2	1.81±0.04	2
	^{214}Bi	1194 s	609.3	46.1	0.330±0.005	0.4
	^{214}Bi	1194 s	1764.5	15.4	0.15±0.005	0.8
	^{214}Pb	295.2 s	295.2	19.3	0.78±0.01	0.7
	^{214}Pb	295.2 s	351.9	37.6	0.658±0.007	0.4
	^{226}Ra	1600 y	186.2	3.6	0.93±0.03	5
	^{230}Th	75,380 y	67.7	0.38	1.9±0.1	22
	^{234m}Pa	70.2 s	1001.0	0.84	0.28±0.05	18
	^{234}Th	24.1 d	63.3	4.8	1.50±0.03	2
	^{234}Th	24.1 d	112.8	0.28	1.2±0.4	52
-	^{108m}Ag	418 y	614.3	89.8	0.257±0.003	0.2
-	^{108m}Ag	418 y	722.9	90.8	0.214±0.002	0.2
-	^{137}Cs	30.07 y	661.7	85.1	0.373±0.003	0.1
-	^{207}Bi	31.55	1063.7	74.5	0.205±0.002	0.3
-	^{241}Am	432.2 y	59.5	35.9	1.87±0.01	0.2
-	^{40}K	$1.277\cdot10^{9}$ y	1460.8	11.0	0.174±0.006	1
-	^{7}Be	53.12 d	477.6	10.52	0.50±0.01	2

Tab. S2 Details about the γ-emissions used in this work. Detection absolute efficiency is the absolute efficiency of the instrumental apparatus, it considers the intrinsic detector efficiency, sample geometry and composition and self-absorption processes. Nuclear data from Chu et al. (1999).

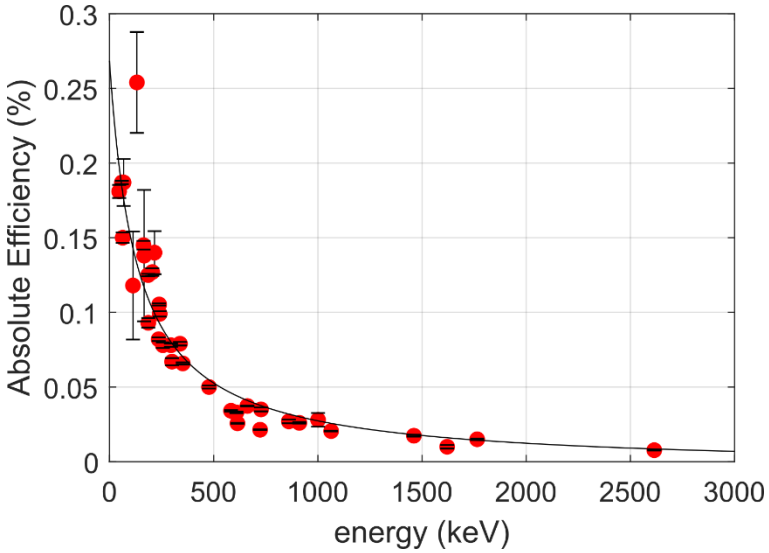

Fig. S2 The absolute detection efficiency of the considered instrumental apparatus. Data have been calculated via Monte Carlo simulations (CUORE collaboration, 2017). Points represent the γ-energies used in this work.

	Analyte	CR-1	CR-2	CR-3	CR-4	CR-5	CR-6	CR-7	CR-Ref
^{235}U chain *(Bq kg^{-1})*	**^{235}U**	2±1	2±2	2.7±0.5	7±3	3±1	2±2	3±1	2.9±0.3
	^{227}Th	2.0±0.4	7±4	3.1±0.4	2.9±0.7	2.9±0.5	3.4±0.5	3.3±0.7	3.3±0.3
^{238}U chain *(Bq kg^{-1})*	**^{234}Th**	38±3	50±7	62±5	44±4	54±5	58±5	62±5	54±4
	^{234m}Pa	34±8	60±30	85±20	49±16	51±20	71±18	74±17	70±16
	^{230}Th	< 37	59±22	50±10	42±12	73±15	69±13	78±22	58±11
	^{226}Ra	41±15	72±83	95±25	44±19	50±22	116±64	75±32	78±15
	^{214}Pb	37±2	48±4	63±3	44±2	50±3	57±3	64±3	57±3
	^{214}Bi	37±2	46±5	62±3	42±3	50±3	55±3	62±3	57±3
	^{210}Pb$_{tot}$	1,299±97	973±98	1,651±123	1,684±132	2,073±159	2,606±199	1,863±139	53±4
^{232}Th chain *(Bq kg^{-1})*	**^{228}Ac**	28±1	37±3	49±3	31±2	35±2	42±2	50±3	44±2
	^{224}Ra	30±3	39±7	55±4	35±4	40±4	47±4	51±4	45±3
	^{212}Pb	28±1	40±4	52±3	35±2	41±2	47±3	50±3	46±2
	^{212}Bi	30±3	43±7	52±4	29±4	35±4	44±4	52±4	45±4
	^{208}Tl	30±1	37±4	51±2	36±2	40±2	45±2	51±2	47±2
single nuclides *(Bq kg^{-1})*	**^{7}Be**	51±23	1,197±173	< 24	1,426±126	1,794±147	1,261±111	< 28	40±23
	^{40}K	504±23	778±86	772±65	551±50	635±55	714±61	739±62	852±72
	^{108m}Ag	< 0.2	0.8±0.4	< 0.2	< 0.2	< 0.2	0.3±0.1	0.45±0.08	< 0.02
	^{137}Cs	478±28	45±5	581±34	172±12	235±15	628±40	3,048±181	0.89±0.09
	^{207}Bi	0.8±0.1	< 0.3	1.2±0.2	0.6±0.2	0.6±0.2	1.4±0.3	6.3±0.5	< 0.3
	^{241}Am	3.8±0.3	0.4±0.2	6.2±0.4	0.9±0.2	3.1±0.3	8.7±0.6	40±2	< 0.2
carbonaceous content *(% m/m)*	**organic carbon**	4.4±0.2	2.2±0.1	2.2±0.1	3.4±0.2	4.9±0.2	3.6±0.2	2.5±0.1	0.45±0.02
	elemental carbon	0.43±0.02	0.097±0.005	0.31±0.02	0.20±0.01	0.39±0.02	0.34±0.02	1.03±0.05	< 0.01

Tab. S3 Full data concerning the samples considered in this work. For each sample activity concentrations of radionuclides and mass concentration of carbonaceous species are reported.

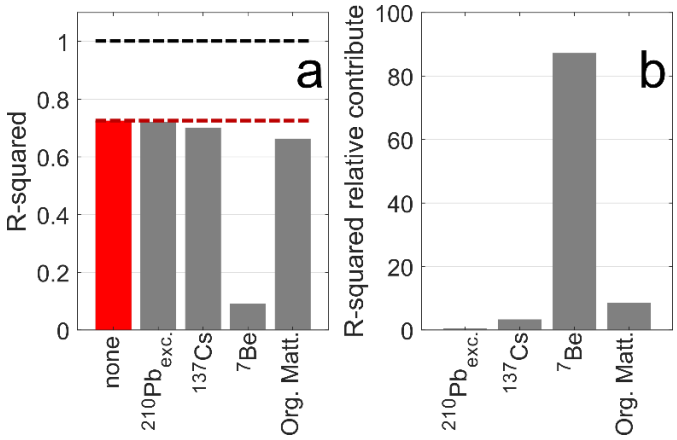

Fig. S3 Results from multiple linear regression applied as a classification tool on cryoconite samples. Only the variables presenting significant differences considering cryoconite types have been considered, they are: $^{210}Pb_{exc.}$, ^{137}Cs, ^{7}Be and organic matter (OM). Panel a shows the R-squared associated with the calculated models. The red bar refers to the model obtained when all variables are included, and grey bars refer to models calculated by excluding single variables (indicated in x-axes labels). Panel b refers to the relative role of single variables with respect to the complete model.

References

Chu, S.Y.F., Ekstrom, L.P., Firestone, R.B. 1999. The Lund/LBNL Nuclear Data Search. [Online], Available at: www.nucleardata.nuclear.lu.se/toi.

CUORE collaboration. 2017. The projected background for the CUORE experiment. Eur. Phys. J C 77, 543.